Electronic Supplementary Material (ESI) for Lab on a Chip.

Centrifugal step emulsification applied for absolute quantification of nucleic acids by digital droplet RPA

Supplementary information

Friedrich Schuler[a,b,*], *Frank Schwemmer*[b], *Martin Trotter*[a], *Simon Wadle*[b], *Roland Zengerle*[a,b,c], *Felix von Stetten*[a,b], *Nils Paust*[a,b]

[a] Hahn-Schickard, Georges-Koehler-Allee 103, 79110 Freiburg, Germany

[b] Laboratory for MEMS Applications, IMTEK - Department of Microsystems Engineering, University of Freiburg, Georges-Koehler-Allee 103, 79110 Freiburg, Germany

[c] BIOSS- Centre for Biological Signalling Studies, University of Freiburg, Freiburg, Germany

* Friedrich.Schuler@Hahn-Schickard.de, Phone +49 761 20373208, Fax: +49 761 203-73299

Supplementary Information

The supplementary information will give a more detailed explanation of the process of step emulsification. The influence of the terrace length will be discussed in depth. Finally, more detail is given on structures used for parallelization.

Process of step emulsification and influence of terrace length

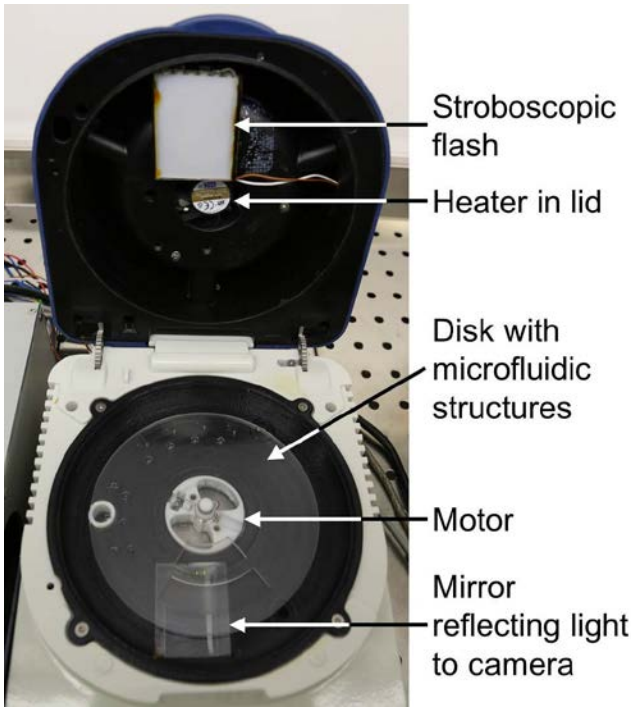

Fig. S 1. Photographic image of microfluidic disk in the open centrifugal setup. The PMMA disk with microfluidic structures is connected to a motor unit that rotates the disk at a given frequency. The lid features a heater to heat the sample to 39 °C, which is needed to perform the digital recombinase polymerase amplification (dRPA). A stroboscopic flash in the lid will irradiate an area of the disk upon each pass during rotation (triggered by a build in switch connected to the rotor). The mirror reflects the light to a camera which is placed to the right of the player setup (not in the picture).

The process of step emulsification is explained in Fig. S 2.

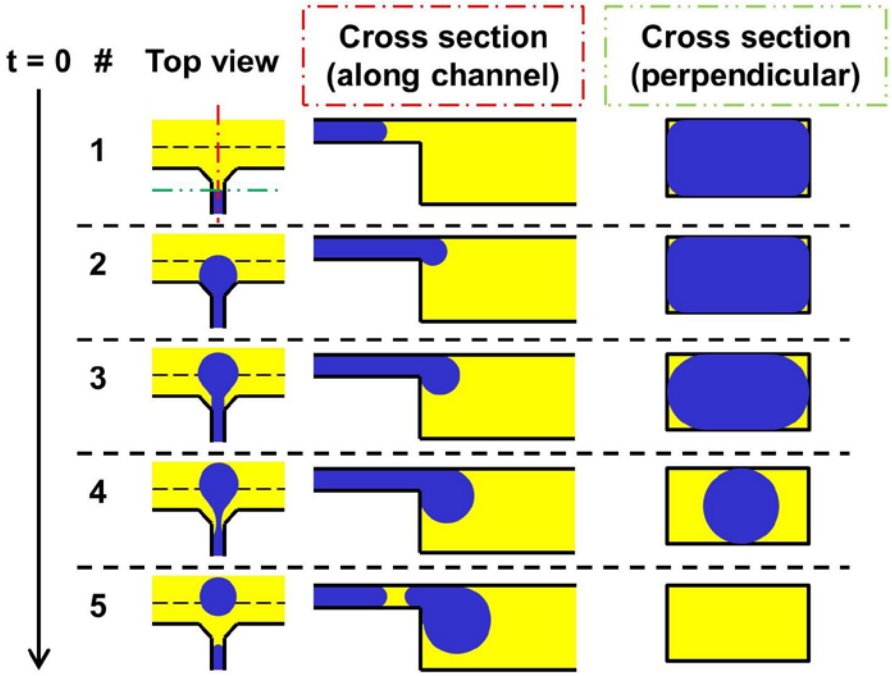

Fig. S 2. The mechanism of step emulsification. Each line shows a top view of the nozzle (left), a cross-section along the channel axis (middle) and a cross-section perpendicular to the channel (right). The five lines show the system at five different states. (1) The aqueous liquid (blue) progresses through the channel but does not wet the walls, as an oil film remains between the aqueous phase and the walls. The gutters of the channel are filled with oil (yellow). (2) The aqueous liquid advances to the terrace and spreads out. Most of the volume is still confined by the ceiling and the bottom but parts of the volume begin to spread across the edge of the terrace. (3) As the liquid pushes forward over the edge of the terrace, the curvature of the interface and thus the capillary pressure in the forming droplet reduces drastically. Since the liquid on top of the terrace and in the channel is confined by the structure, the surface curvature and thus capillary pressure in this region is significantly higher causing a pressure gradient in the aqueous phase across the edge of the terrace. Along the pressure gradient, the liquid flows off the terrace. Consequently, the drop outside the terrace grows further, surface curvature reduces and the pressure gradient increases. As the liquid flow across the edge of the terrace is higher than the supply flow rate in the channel, the cross-section of the aqueous thread reduces (4) As the thread continues to shrink, it first detaches from the side walls of the channel and then from bottom and ceiling. As the thread is no longer confined by any two walls, it becomes instable and quickly ruptures due to Raleigh-Plateau instabilities.

The influence of terrace length on the droplet diameter was evaluated as well. The results can be seen in Fig. S 3.

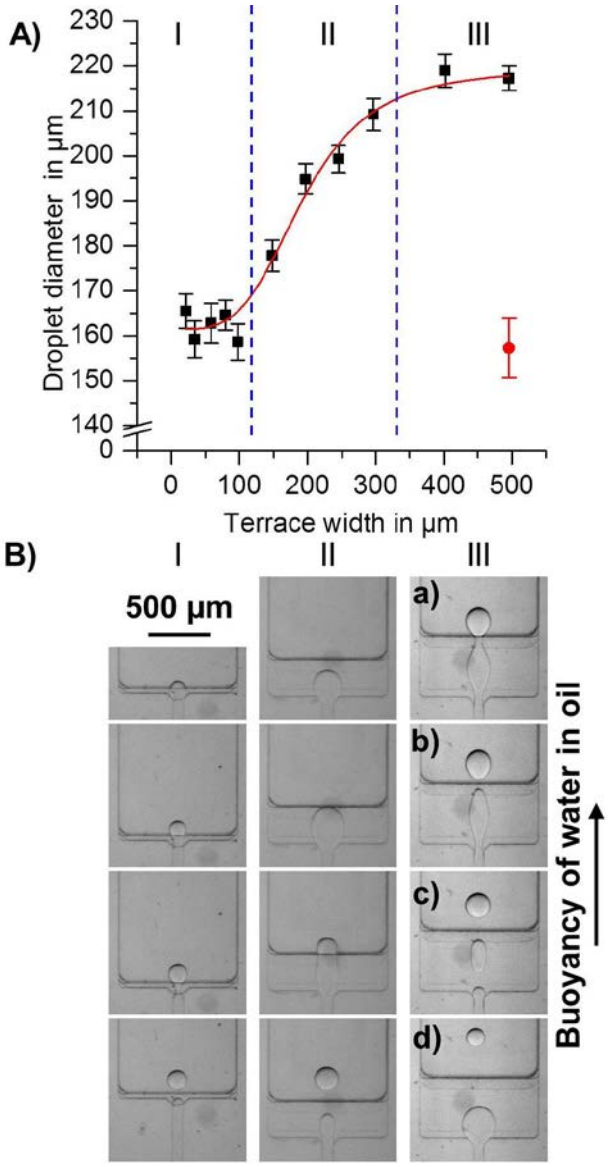

Fig. S 3. Influence of terrace length on droplet diameter.

A) The droplet diameter increases with increasing terrace width. The curve can be divided in three domains (I-III). Domain I: Channel dimensions dominate droplet diameter as the terrace width is smaller than the channel width. Domain II: The influence of terrace length on the droplet diameter becomes dominating as the terrace width becomes larger than the channel width. Domain III: The buoyancy driven formation of the droplet becomes dominant, influencing droplet break-up. At a critical length of 500 µm terrace length, satellite droplets develop and two distinct populations are observed (red circle and black square). Each data point corresponds to 20 independent measurements of droplet diameter. The channel depth and width are constant at 60 µm and 90 µm, respectively. Error bars given are standard deviations (SD).

B) Droplet break-up for the three domains. I) Terrace length has no influence on droplet diameter since the length is short compared to the channel width. II) The terrace length dominates the droplet

diameter. III) Buoyancy dominates the droplet diameter. When the terrace length becomes long compared to the droplet diameter, populations of droplets with two different diameters are produced. The mechanism for this is shown in the image sequence above: (a) The first (larger) droplet is being formed by the first constriction at the step. A second constriction closer to the nozzle can be observed with a bulge of liquid in between the two constrictions. (b) The first droplet detaches from the main liquid thread while the second constriction narrows. (c) A second (smaller) droplet is formed on the terrace. (d) The second smaller droplet rises to the collection chamber.

For terrace lengths that are small compared to the channel width, a droplet dependency on the terrace length could not be identified (domain I). Here, as the liquid thread spreads across the terrace, the capillary counter pressure increases until the aqueous phase forms a half-spherical like shape (from top view). The dominating dimension for the half-spherical like shape and thus for the maximum counter pressure is the channel width, thus the influence of the terrace length is negligible in this regime.

As the terrace length exceeds the channel width, the droplet diameter increases with increasing terrace length (domain II). After having exceeded the half-spherical like shape, the droplet grows until its meniscus reaches the terrace edge and breaks-up due to the abrupt decrease of capillary pressure as the meniscus spreads over the terrace edge.

As the terrace length increases even further, buoyancy between the aqueous and the oil phase starts to gain influence on droplet formation (domain III). The buoyancy causes a deformation of the droplet that forms on the terrace. The droplet shape is not spherical anymore but gains a tear-drop like shape (Fig. S 4). Since the volume of this tear-drop like shape is smaller than that of the corresponding spherical shaped droplet, the volume increase of formed droplets slows down for increasing terrace lengths.

As the terrace length exceeds a critical value (in our configuration 500 µm), the droplet volume does not increase with larger terrace lengths. In this configuration, the forming tear-drop like droplet on the terrace is close to break-up on the terrace due to centrifugal gravity forces. Therefore, the contribution of the capillary pressure driven break-up mechanism is reduced in favor of a gravity driven break-up. This can lead to the formation of satellite droplets as shown in Fig. S 3 A) and B). A structure with a very long terrace was designed in order to show the buoyancy driven formation of the tear-drop like droplet on the terrace as shown in Fig. S 4.

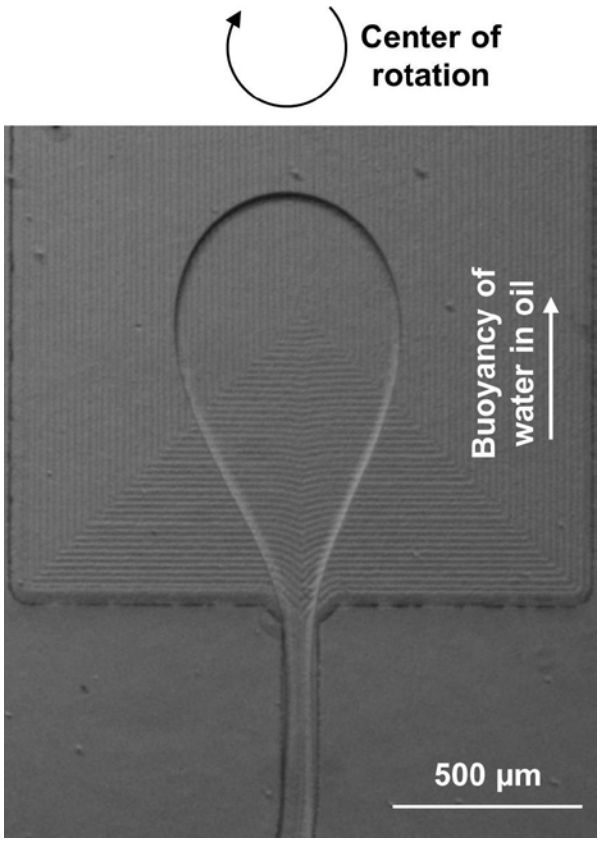

Fig. S 4. Microscopic image of tear-drop like droplet formed on the terrace. The water droplet (ρ=1) in oil (ρ=1.6) is deformed due to buoyancy in the centrifugal gravity field.

Parallelization and high throughput

To evaluate the possibility of parallelization, a design with two nozzles leading to the same chamber was prepared as can be seen in Fig. S 5. The number of droplets produced in a given time interval was the same for the left and the right nozzle and the droplet diameter did not differ, either.

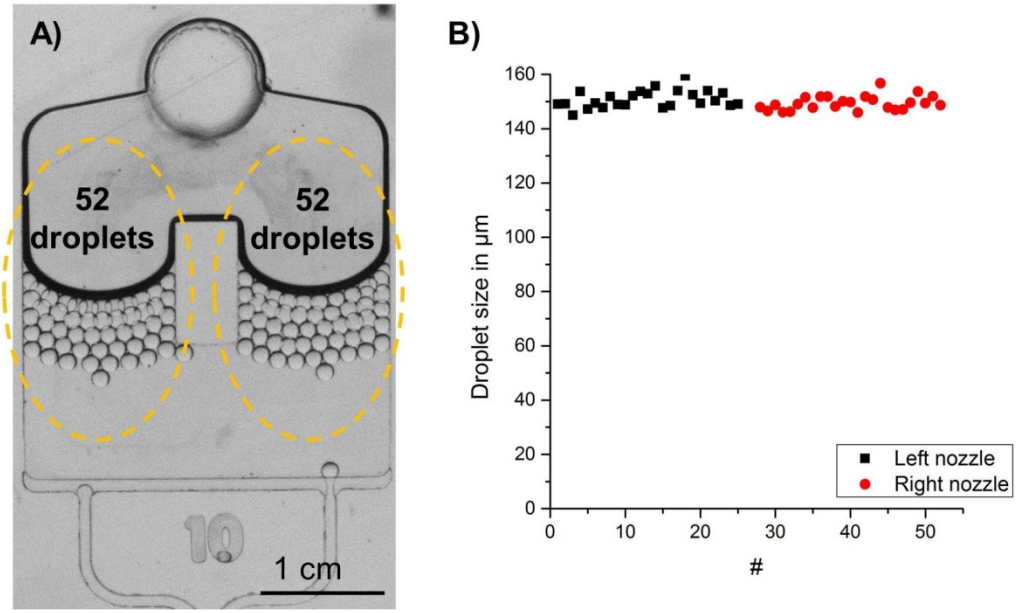

Fig. S 5. Parallelization with two nozzles.
A) Microscopic image of a two-nozzle setup. The channel branches in two smaller channels with half the cross section of the main channel. Each of the channels leads to a separate nozzle. Both nozzles produce droplets at the same frequency.
B) Droplet diameter in µm is given for the left and right nozzle (black squares and red circles respectively). No difference in droplet diameter can be observed.

In order to increase the throughput, one medium throughput structure (see Fig. S 6) was designed to perform digital droplet RPA (compare Fig. 5 A)). The nozzle geometry was: nozzle width 90 µm, nozzle depth 60 µm, terrace length 100 µm. As multiple nozzles are fed from one feed channel (green), the pressure along the feed channel drops at each nozzle (since the pressure is partly released by the formation of droplets at the end of the nozzle). This leads to a low pressure at the latter nozzles and therefore to a low droplet generation frequency. In order to ensure high droplet generation frequencies for all nozzles, the feed channel had a much smaller fluidic resistance then the nozzles (i.e. a larger cross section). For the medium throughput structure (see Fig. S 6) one feed channel for all 23 nozzles was chosen. However, to feed the 72 nozzles 8 groups of 9 nozzles each were designed, all fed by an individual feed channel. The 8 feed channels were connected to the joined feed channel by Y-junctions. At each Y-junction, the sum of the cross sections for the two branching channels was the same as the cross section of the feeding channel.

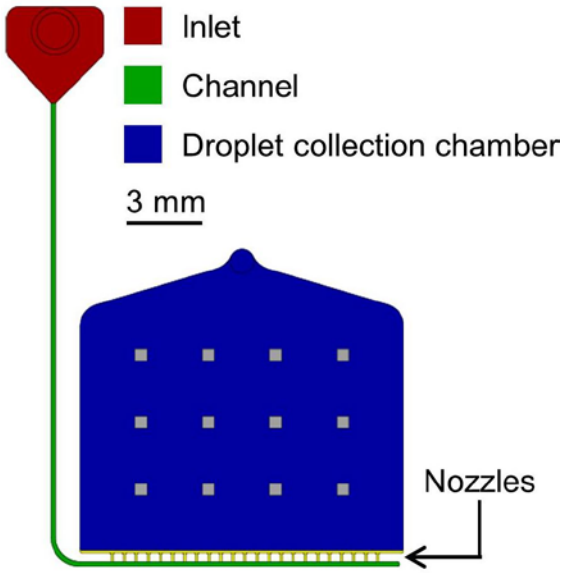

Fig. S 6. Top view of a CAD sketches of structures used for centrifugal step emulsification.

Droplet generation structure with 23 nozzles for medium throughput. The chamber has three rows of four pillars each supporting the sealing foil. The shallow chamber is required to generate monolayers of droplets for readout of the digital RPA.

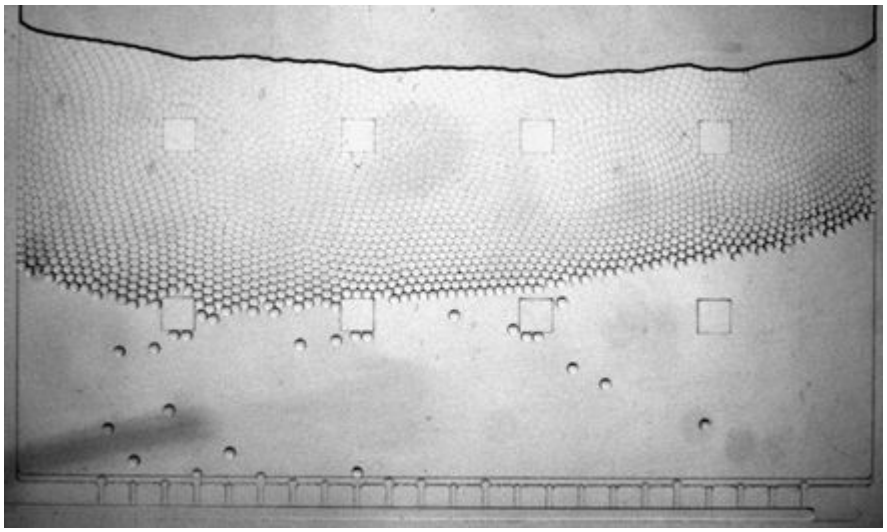

Movie S 1 Showing medium throughput droplet production in real time. Droplet are being produced by 23 nozzles (seen on the bottom) simultaneously. Due to buoyancy the rise in the oil filled chamber. The top part of the chamber is filled with air. The 8 squares in the image are supporting pillars, which avoid sealing foil lamination to the bottom of the chamber.

The exact sizes of the structures are given in Table S 1.

Table S 1 Feature sizes of the two structures shown in Fig. S 6. The inlet channel in structure B) changes width and depth at every junction (width is halved) and before every junction (width is converted to depth and vice versa). The aspect ratio is kept constant at 1.4 and 0.7 respectively.

Feature	Size
Structure Fig. S 6	
Inlet chamber volume	ca. 17 µl
Channel width	200 µm
Channel depth	100 µm
Nozzle width	90 µm
Nozzle depth	60 µm
Terrace length	100 µm
Number of nozzles	23
Droplet collection chamber width	13.5 mm
Droplet collection chamber length	10 mm
Droplet collection chamber depth	200 µm
Pillar width/length	500 µm